CONSISTENT EMPIRICAL PHYSICAL FORMULAS FOR POTENTIAL ENERGY CURVES OF $^{38-66}$Ti ISOTOPES BY USING NEURAL NETWORKS

S. Akkoyun [a, 1], *T. Bayram* [b, 2], *S. O. Kara* [c, 3], *N. Yildiz* [a, 4]

[a] Department of Physics, Cumhuriyet University, Sivas, Turkey

[b] Department of Physics, Sinop University, Sinop, Turkey

[c] Department of Physics, Nigde University, Nigde, Turkey

Nuclear shape transition has been actively studied in the past decade. In particular, the understanding of this phenomenon from a microscopic point of view is of great importance. Because of this reason, many works have been employed to investigate shape phase transition in nuclei within the relativistic and nonrelativistic mean field models by examining potential energy curves (PECs). In this paper, by using layered feed-forward neural networks (LFNNs), we have constructed consistent empirical physical formulas (EPFs) for the PECs of $^{38-66}$Ti calculated by the Hartree–Fock–Bogoliubov (HFB) method with SLy4 Skyrme forces. It has been seen that the PECs obtained by neural network method are compatible with those of HFB calculations.

В последнее время активно изучаются ядерные переходы, связанные с формой ядра. В частности, большой интерес вызывает понимание этого феномена с микроскопической точки зрения. По этой причине множество работ посвящено исследованию ядерных фазовых переходов, связанных с формой ядра, в рамках релятивистских и нерелятивистских моделей среднего поля путем изучения уровней потенциальной энергии (УПЭ). В настоящей работе строятся последовательные эмпирические физические формулы для УПЭ изотопов $^{38-66}$Ti, рассчитанные методом Хартри–Фока–Боголюбова с SLy4-силами Скирма с помощью «layered feed-forward» нейронных сетей. Показано, что УПЭ, полученные с использованием нейронных сетей, совместимы с рассчитанными методом Хартри–Фока–Боголюбова.

PACS: 32.10.Bi; 87.18.Sn

INTRODUCTION

The study of the structural evolution in atomic nuclei with changing numbers of their neutron and proton constituents dates back to the early days of the nuclear physics. In the last decade, a number of theoretical developments have given insights into, and ways to model, this structural evolution, particularly in transitional regions of rapid change [1, 2]. These

[1] E-mail: sakkoyun@cumhuriyet.edu.tr
[2] E-mail: tbayram@sinop.edu.tr
[3] E-mail: sokara@science.ankara.edu.tr
[4] E-mail: nyildiz@cumhuriyet.edu.tr

864 *Akkoyun S. et al.*

breakthroughs involve the concepts of quantum phase transitions (QPTs) and the critical-point symmetries. A new class of symmetries $E(5)$ and $X(5)$ have been suggested to describe shape phase transitions in atomic nuclei by Iachello [3, 4]. The $E(5)$ critical-point symmetry has been found to correspond to the second-order transition between $U(5)$ and $O(6)$, while the $X(5)$ critical-point symmetry has been found to correspond to the first-order transition between $U(5)$ and $SU(3)$. These symmetries were experimentally identified in the spectrum of ^{134}Ba [5] and ^{152}Sm [6].

From theoretical point of view, QPTs have been studied within the Interacting Boson Model (IBM) and the solutions of Bohr–Mottelson differential equations. They are useful representations for describing QPTs in nuclei. Also, phenomenological mean field models, e.g., Hartree–Fock–Bogoliubov (HFB) method [7, 8] and relativistic mean field (RMF) model [9–11] have been used to investigate the critical-point nuclei with $E(5)$ or $X(5)$ symmetry in [12–20]. In these studies, potential energy curves (PECs) obtained from quadrupole constrained calculations have been used for describing the possible critical-point nuclei. Relatively flat PECs are obtained for critical-point nuclei with $E(5)$ symmetry, while in nuclei with $X(5)$ symmetry, PECs with a bump are obtained. It should be noted, however, that one should go beyond a simple mean field level for a quantitative analysis of QPT in nuclei. For this purpose, some methods have been utilized in [21–24]. The application of these methods for a systematic study of QPT in nuclei is at present still very time-consuming. Therefore, the evolution of the PECs along the isotopic or isotonic chains is important and can be used for qualitative understanding of QPTs in nuclei.

In [19], the HFB method with SLy4 Skyrme forces has been employed to investigate ground-state properties of even–even $^{38-66}$Ti isotopes. The calculated binding energies and deformations with the Skyrme force were obtained in good agreement with the available experimental data. In particular, shape evolution of Ti isotopes has been investigated by using calculated PECs to search for $E(5)$ symmetry in Ti isotopes, together with the neutron single-particle levels. Particularly, ^{46}Ti has been suggested as possible critical-point nucleus with $E(5)$ symmetry.

Recently, neural networks have emerged with successful applications in many fields, obtaining potential energy surfaces [25], studying nuclear mass systematics [26], investigating nucleon separation energies [27], classifying unknown energy levels [28], estimating the density functional theory energy [29], investigating ground-state geometries [30], mapping potential energy surfaces [31], determination of beta decay half-lives [32], and identifying impact parameter in heavy-ion collisions [33]. In this work, borrowing data from our previous work [19], the PECs for $^{38-66}$Ti isotopes as a function of quadrupole deformation parameter (β_2) were obtained by using layered feed-forward neural networks (LFNNs).

Due to the physical phenomena correlated with potential energy curves (PECs) of the isotopes are characteristically highly nonlinear, it may be difficult to construct empirical physical formulas (EPFs) for binding energy functions. By appropriate operations of mathematical analysis, derivation of highly nonlinear physical functions for binding energies is of utmost interest. These EPFs would be used for specific purposes in analyzing PECs. We particularly aim to construct explicit mathematical functional form of LFNN–EPFs for PECs. While the PECs were intrinsically nonlinear, even so training set LFNN–EPFs successfully fitted these binding energies. Furthermore, test set LFNN–EPFs consistently predicted the binding energies. That is, the physical laws embedded in the data were extracted by the LFNN–EPFs.

The letter is organized as follows. In Sec. 1, the HFB method and numerical details are given briefly. In Sec. 2, details on artificial neural networks are given. The results of this study and discussions are presented in Sec. 3. Finally, conclusions are given in Sec. 4.

1. HFB FORMALISM AND NUMERICAL DETAILS

In the HFB method, many properties of the nuclei can be described in terms of a model of independent particles which move in an average potential. In the HFB formalism, a two-body Hamiltonian of a system of fermions can be interpreted in terms of a set of annihilation and creation operators. The ground-state wave function is described as the quasi-particle vacuum and the linear Bogoliubov transformation provides connection between the quasi-particle operators and the original particle operators. The basic building blocks of the HFB method are the density matrix and the pairing tensor, and expectation value of the HFB Hamiltonian could be expressed as energy functional (details can be found in [8, 34]). In terms of Skyrme forces, the HFB energy has the form of local energy density functional which contains the sum of the mean field and pairing energy densities. These fields can be calculated in the coordinate space [8, 34].

In this work, input data for construction of empirical formula of the PECs obtained from constrained HFB calculations with SLy4 Skyrme force for Ti isotopes was taken from [19]. In this reference, HFB equations have been solved by expanding quasi-particle wave functions on a harmonic oscillator basis expressed in coordinate space. For pairing, the Lipkin–Nogami method was implemented by performing the HFB calculations with an additional term included in the HF Hamiltonian. Further details on choosing of oscillator bases and parameters can be found in [19].

2. ARTIFICIAL NEURAL NETWORKS

Artificial neural networks (ANNs) are known to be very powerful multivariate tools that are used when standard techniques fail to properly take account of the correlation between these variables. The typical goal of the ANN is to get a fast function, which models well the output of complicated and CPU consuming data. Since trained network is very fast and uses neither much memory nor CPU, ANN is well suited for this task. ANNs offer several advantages, requiring less formal statistical training, ability to detect complex highly nonlinear relationships between input and output variables, ability to detect all possible interactions between predictor variables. Another benefit of the ANNs appears in case of existing dataset with a high percentage of missing data.

ANNs are mathematical models that mimic the human brain. They consist of several processing units called neurons which have adaptive synaptic weights [35]. ANNs are also effective tools for pattern recognition. The LFNN which is particular kind of ANN consists of three layers: input, hidden and output (Fig. 1). The number of hidden layers can differ, but a single hidden layer is enough for efficient nonlinear function approximation [36]. In this study, one input layer with one neuron ($p = 1$), one hidden layer with many (h) neurons and one output layer with one neuron ($r = 1$) LFNN topology was used for accurate and reliable prediction of the binding energies for even–even $^{38-66}$Ti isotopes. Analyses were performed for different hidden neuron numbers.
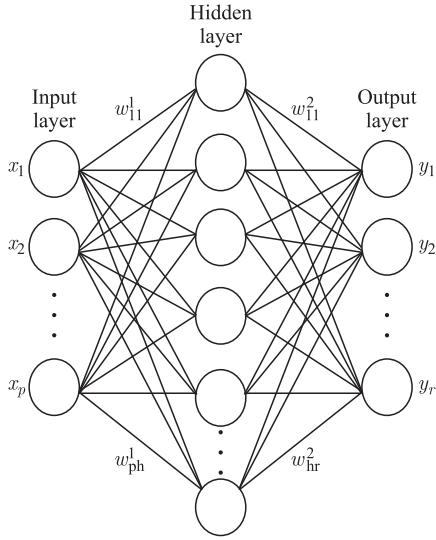
Fig. 1.   Fully connected one input–one hidden–one output layer LFNN. $x_i (i = 1, \ldots, p)$ and $y_i (i = 1, \ldots, r)$ are input and output vector components, respectively. w^i_{jk} is weight vector component, where i is a layer index, jk weight component from the jth neuron of ith layer and kth neuron of $(i + 1)$th layer

The neuron in the input layer collects the data from environment and transmits via weighted connections to the neurons of hidden layer which is needed to approximate any nonlinear function. The hidden neuron activation function can be theoretically any well-behaved nonlinear function. In this work, the type of activation function was chosen hyperbolic tangent for hidden layer. Finally, the output layer neuron returns the signal after the analysis. Note that an input layer with single neuron is firmly equivalent to one neuron LFNN with an appropriate activation function. As far as the activation function is analytical, the output is also an analytical function of the input.

Neural network software NeuroSolutions v6.02 was used [37]. The LFNN inputs were quadrupole deformation parameters (β_2) for $^{38-66}$Ti isotopes and the desired outputs were binding energies. As mentioned before, these data for both training and test phases were borrowed from our previous work [19]. For all LFNN processing case, whole data were divided into two separate sets, 75% for the training phase and 25% for the test phase. In the training phase, Levenberg–Marquardt back-propagation algorithm [38, 39] was used for the training of the LFNN. By convenient modifications, LFNN modifies its weights until an acceptable error level between predicted and desired outputs is attained. The error function which measures the difference between outputs was mean square error (MSE) given as

$$\text{MSE} = \left[\sum_{k=1}^{r} \sum_{i=1}^{N} (y_{ki} - f_{ki})^2 \right] \Big/ N, \tag{1}$$

where N is the number of training and test samples, whichever applies.

Then by using LFNN with final weights, the performance of the network is tested over an unseen data. If the predictions of the test dataset are good enough, the LFNN is considered to have consistently learned the functional relationship between input and output data [40]. In this study, for different h numbers, the minimum MSE values were given in Subsec. 3.2.

2.1. The Concrete Algorithm for Detector Response LFNN–EPF Construction. Due to the well-established fact that a single hidden layer LFNN is enough for efficient nonlinear function approximation [36], in this paper single hidden layer LFNNs were used. For simplicity, only the single hidden layer LFNN functionality is explained. Borrowing from [36], for a single hidden layer LFNN, in Fig. 1, the desired output vector $\mathbf{y}$ is approximated by a network multioutput vector $\mathbf{f}$ which is defined as

$$\mathbf{f} : R^p \to R^r : \mathbf{f}_k(\mathbf{x}) = \sum_{j=1}^{h_1} \beta_{jk} G(A_j(\mathbf{x})), \ x \epsilon R^p, \ \beta_{jk} \epsilon R, \ A_j \epsilon A^p, \quad \text{and} \quad k = 1, \ldots, r, \tag{2}$$

where $\mathbf{x}$ is the LFNN input vector in Fig. 1; A^p is the set of all functions of $R^p \to R^r$ defined by $A(\mathbf{x}) = \mathbf{w} \cdot \mathbf{x} + b$; $\mathbf{w}$ is input to hidden layer weight vector and b is the bias weight. In Fig. 1, the columns of the weight matrices $\mathbf{w}^1$ and $\mathbf{w}^2$ correspond to weight vectors defined in $A(\mathbf{x})$ and β in Eq. (2). However, as can be seen in Fig. 1 and Eq. (2), the correspondences $\mathbf{w}^1 \to A(\mathbf{x})$ and $\mathbf{w}^2 \to \beta$ are valid only for single hidden layer LFNN. Another point is that, in Eq. (2), the hidden neuron activation function $G : R \to R$ can be theoretically any well-behaved nonlinear function, proving that an LFNN is a universal nonlinear function approximator. In applications, G is often chosen as a kind of nonlinear sigmoid function.

In this work, the type of activation function G in Eq. (2) was hyperbolic tangent ($\tanh = (e^x - e^{-x})/(e^x + e^{-x})$) for hidden layer and linear for output layer. For LFNN fitting of the binding energy (output) versus input, one input layer neuron ($p = 1$), one output layer neuron ($r = 1$) and one hidden layer of $h_1 = 4, 9,$ and 14 hidden neurons were used. The total number of adjustable weights ($p \times h_1 + h_1 \times r = h_1 \times (p + r) = h_1 \times (1 + 1) = 2h_1$) was 8, 18, and 28.

2.2. Final $f_{\min}$ Details. In this paper, LFNN input vector $\mathbf{x}$ was the quadrupole deformation parameters and desired vector $\mathbf{y}$ was binding energies. $\mathbf{f}_{\min}$ totally depends on the structure of the network output vector function $\mathbf{f}$ and the final weight vector $\mathbf{w}_f$. In (2), components of the weight are embedded in $A(\mathbf{x})$ and β. The $\mathbf{f}$ depends on the explicit forms of G and A functions in (2). In this paper, setting $\beta = \mathbf{w}^1$ in Fig. 1, G is nonlinear tangent hyperbolic and A is the dot product of $\mathbf{w}^1$ and $\mathbf{x}$ in Fig. 1. So, we can construct explicit form of $\mathbf{f}$. Afterwards, by minimization of MSE values of Eq. (1), we finally obtain $\mathbf{f}_{\min} = \mathbf{f}(\mathbf{w}_f)$. Now, the concrete LFNN–EPF construction algorithm for nonlinear PECs is completed. Final details for $f_{\min}$ of this paper are given in Sec. 3.

3. RESULTS AND DISCUSSIONS

In figures and text where it suitably applies, the abbreviation *calc* is used for the calculated data obtained by HFB theory. As mentioned in Sec. 2, the LFNN training and test set data used in this paper were borrowed from [19]. Note that the LFNN inputs and outputs used in this paper were explicitly defined in (2). Inputs were quadrupole deformation parameters (β_2) and the corresponding outputs were binding energies of the Ti isotopes. The abbreviation neural network output (nno) is for both training or test set results.

3.1. Training. For the PECs, the training set nno fittings were given in terms of quadrupole deformation parameters (β_2) versus binding energies of the Ti isotopes obtained from SLy4 Skyrme force (Fig. 2). The LFNN had a single hidden layer with $h = 4, 9, 14$. The number of data points belonging to the training phase was 30, which is 75% of overall data. It can be clearly seen in Fig. 2 that ^{42,50,62}Ti isotopes which have shell closure with magic neutron numbers ($N = 20$, $N = 28$) and semi-magic number ($N = 40$) were found to be spherical. Also ^{40}Ti was found to be spherical, while ^{38}Ti has prolate shape. The PECs of ^{44}Ti seem relatively flat with a small bump which means that it is a possible example of β-soft nucleus. The PEC of ^{46}Ti and ^{48}Ti is flat from $\beta_2 = -0.2$ to $\beta_2 = 0.35$ and $\beta_2 = -0.2$ to $\beta_2 = 0.2$, respectively. In both of the PECs, the variations of the total binding energies are less than 2 MeV through these β_2 intervals, which implies that the barriers against deformation are so weak. However, the PECs of ^{46}Ti are much flatter than those of ^{48}Ti and the PECs of ^{48}Ti have a small bump in Fig. 2. This means that ^{46}Ti should be an example of critical-point
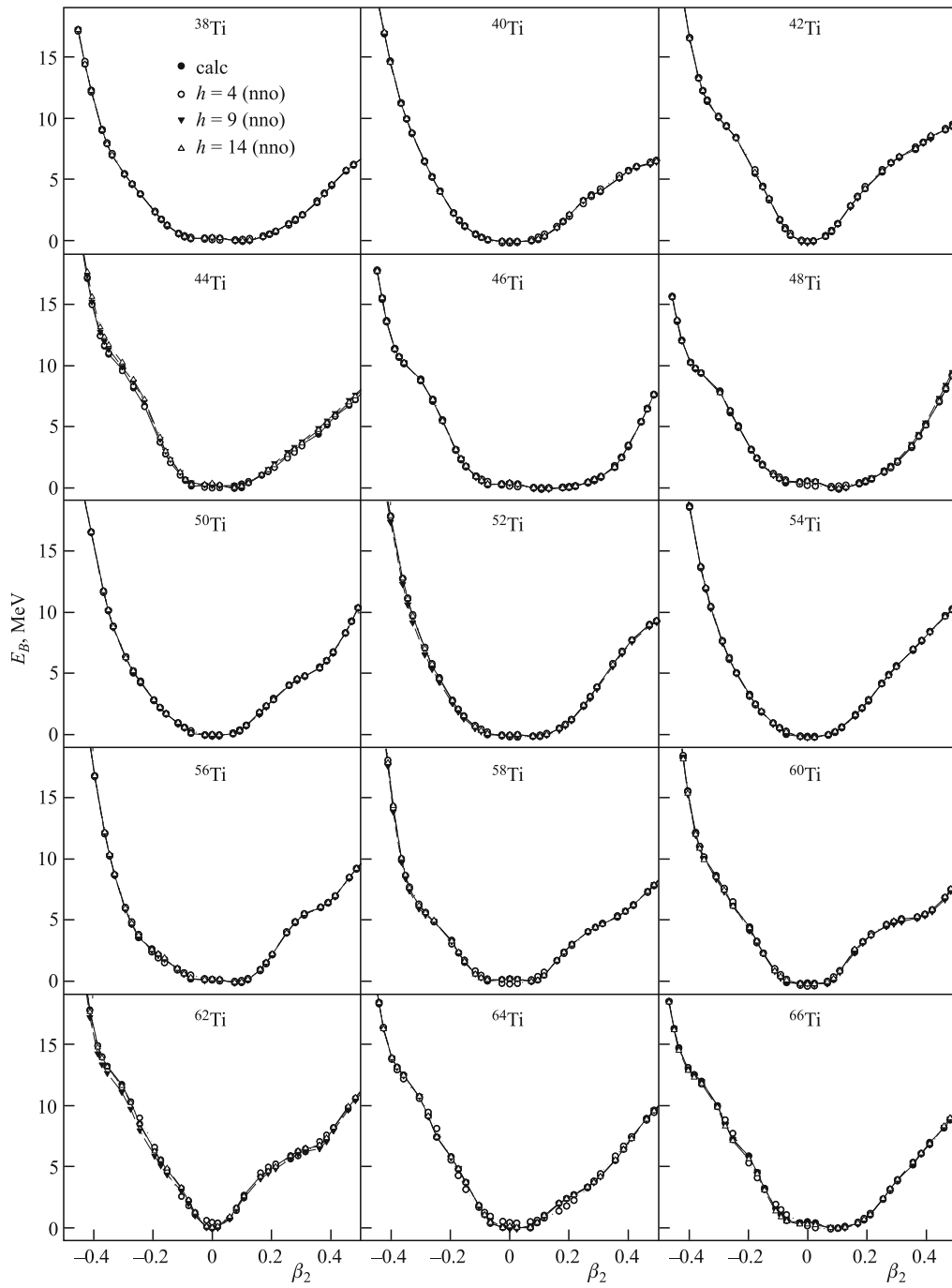
Fig. 2. HFB calculation (calc) with SLy4 Skyrme force and neural network output (nno) training set fittings for PECs of different Ti isotopes

nuclei with $E(5)$ symmetry, while ^{48}Ti can be thought as an example of candidate critical-point nuclei with $X(5)$ symmetry. In addition, $^{54-58}$Ti nuclei have flat PECs with a very small bump, while ^{52}Ti and ^{60}Ti have flat PECs. It is possible to argue that $^{54-58}$Ti can be an example of possible critical-point nuclei with $X(5)$ symmetry, while ^{52}Ti and ^{60}Ti should be candidate for $E(5)$ symmetry. Further details and additional evidence for suggestion of ^{46}Ti nucleus as an example of critical-point nuclei with $E(5)$ symmetry can be found in [19].

Moreover, in the same figures, one would also concentrate only on comparing specific nno fittings with its corresponding calc values. In Fig. 2, the nno fittings agree exceptionally well with highly nonlinear calc values. Particularly note that, as principally aimed in this paper, the obtainment of PECs had been successfully made by the LFNN–EPFs.

3.2. Test Dataset Predictions: Consistency of the EPFs Constructed. Unless the training set LFNN–EPFs are further tested over the data, these fitted EPFs cannot be used consistently over a desired range of the data. In other words, if the training sets LFNNs well predict previously unseen test dataset, then the LFNNs are regarded to have successfully generalized the data, proving consistent estimations. If the estimations are consistent with the test data values, then the LFNNs can be taken as appropriate LFNN–EPFs. The number of data points belonging to the training phase was 10, which is 25% of overall data. For the PECs, the corresponding test set nno predictions in Fig. 2 were given in Fig. 3. As a global criterion of approximation quality of the predictions, the maximum absolute errors (MAE) and the MSE values were given in table for $h = 4, 9, 14$. Naturally, the single hidden layer training set LFNNs with $h = 4, 9, 14$ which led to Fig. 2 were also used for nno test set predictions. As can be seen in Fig. 3, the nno predictions agree exceptionally well with highly nonlinear calc values. This clearly shows that the test set LFNNs of the quadrupole deformation parameters (β_2) versus binding energies of the Ti isotopes have consistently generalized the training LFNN fittings. Therefore, LFNNs obtained can be safely used as LFNN–EPFs because the physical law embedded in the β_2 versus binding energies of the Ti isotopes data has been

MSE and MAE values of test set predictions for $h = 4, 9,$ and 14

| Isotope	$h = 4$		$h = 9$		$h = 14$	
	MSE	MAE	MSE	MAE	MSE	MAE
^{38}Ti	0.0091	0.20	0.0020	0.10	0.0001	0.05
^{40}Ti	0.0260	0.44	0.0028	0.09	0.0061	0.15
^{42}Ti	0.0260	0.34	0.0120	0.23	0.0069	0.15
^{44}Ti	0.0040	0.11	0.0810	0.41	0.1500	0.72
^{46}Ti	0.0072	0.13	0.0037	0.12	0.0036	0.13
^{48}Ti	0.0093	0.17	0.0190	0.27	0.0058	0.15
^{50}Ti	0.0171	0.26	0.0113	0.17	0.0025	0.09
^{52}Ti	0.0151	0.19	0.0774	0.57	0.0042	0.14
^{54}Ti	0.0170	0.23	0.0105	0.19	0.0110	0.20
^{56}Ti	0.0195	0.29	0.0069	0.18	0.0035	0.15
^{58}Ti	0.0470	0.51	0.0260	0.39	0.0073	0.23
^{60}Ti	0.0164	0.23	0.0367	0.38	0.0220	0.30
^{62}Ti	0.0685	0.53	0.1692	0.73	0.0210	0.34
^{64}Ti	0.1330	0.70	0.0152	0.28	0.0075	0.21
^{66}Ti	0.0489	0.44	0.0197	0.27	0.0300	0.42
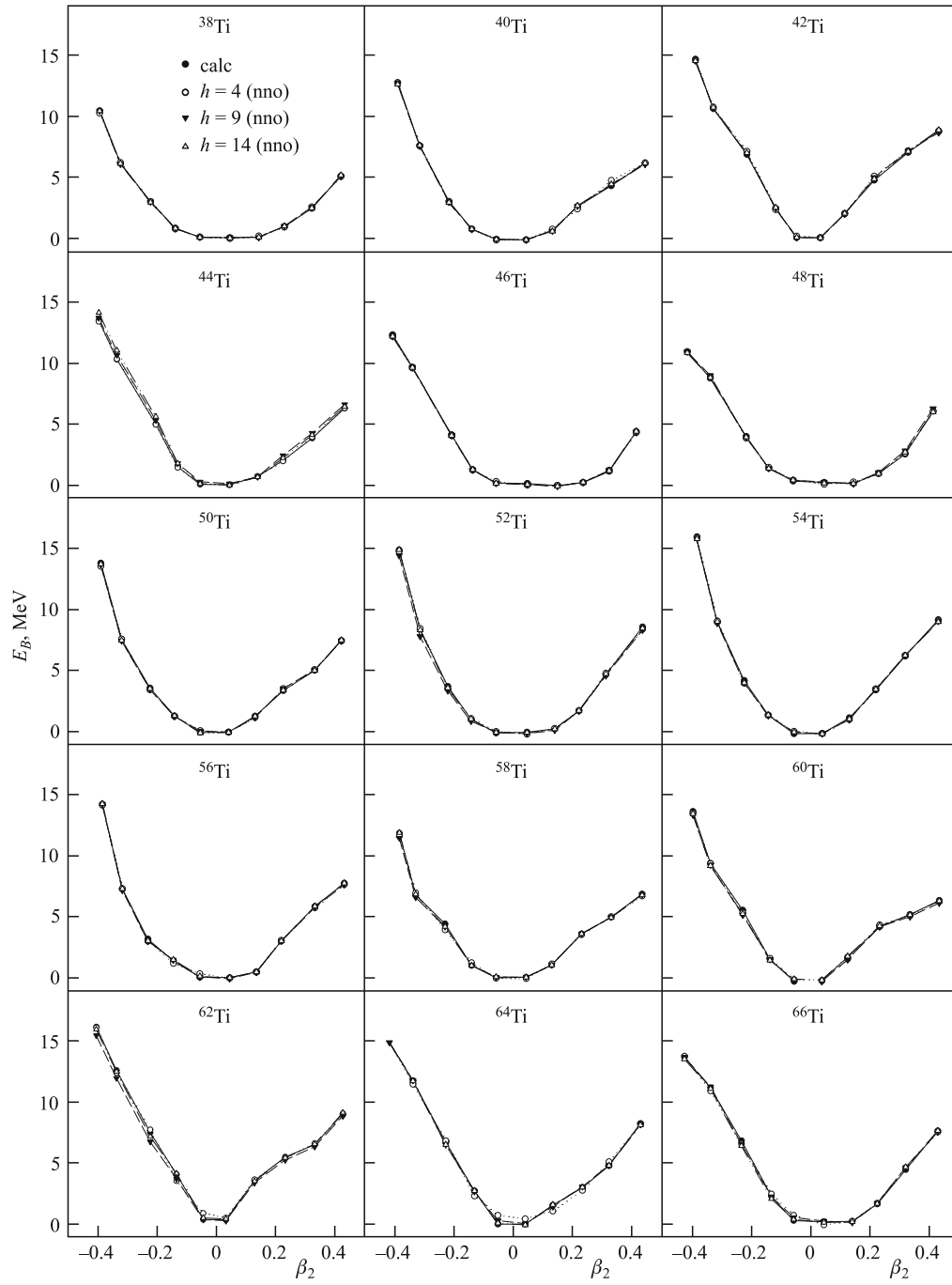
Fig. 3. HFB calculation (calc) with SLy4 Skyrme force and neural network output (nno) test set predictions for PECs of different Ti isotopes

successfully extracted by the LFNN constructed. Particularly note that, as principally aimed in this paper, the PECs have been successfully made by the LFNN–EPFs.

A caution for choosing the optimal h value: for a specified physical application, a specific number of h of LFNN–EPF must be chosen so that the physicist-users can appropriately use the final LFNN–EPF. However, in our paper, for a given potential energy curve, the LFNN–EPF estimation has been done by various values of h ($h = 4, 9, 14$). Still, as explained in detail in [40], there is actually no optimal h for a specific problem. However, as a general rule, as the number of input-output data increases, the number h must be appropriately increased. But, again there is no well-defined h number for the given physical problem which is under study by the LFNN–EPF. In this paper, we have simply chosen relatively low ($h = 4$), medium-size ($h = 9$) and relatively high ($h = 14$) h numbers to make consistent LFNN estimations of the EPFs. As can be seen from Figs. 2, 3 and table, as the number of h increases, the estimations get generally better. However, the estimation improvements with increasing h are rather limited. Therefore, any of h values can be chosen for the final LFNN–EPF, depending on the accuracy level with which the physicist-users are satisfied. But to be more decisive in this issue, we may recommend that the physicist-users should prefer the consistent estimation with the highest h value ($h = 14$) for the sake of improved consistency.

4. CONCLUSIONS AND POTENTIAL APPLICATIONS

In this paper, based on inputs of the PECs obtained from constrained HFB calculations with SLy4 Skyrme force for $^{38-66}$Ti isotopes, we generated PECs distributions by using artificial neural networks. The PECs of nuclei can provide knowledge for qualitative understanding of QPTs in nuclei. These distributions can help determination of the nuclear shapes. It is clearly seen that the neural network method, which can be applied very fast, was consistent with the calculated results. The advantage of the ANN method is that it does not need any relationship between input and output data. For highly nonlinear binding energies for quadrupole deformation parameters (β_2), we have novelly constructed consistent empirical physical formula (EPFs) by appropriate LFNNs. The test set LFNNs of the quadrupole deformation parameters (β_2) versus binding energies of the Ti isotopes have generalized the training LFNN fittings. Therefore, the test set LFNNs can be confidently used as LFNN–EPFs.

REFERENCES

1. *Casten R. F., McCutchan E. A.* Quantum Phase Transitions and Structural Evolution in Nuclei // J. Phys. G: Nucl. Part. Phys. 2007. V. 34. P. R285–R320.
2. *Cejnar P., Jolie J., Casten R. F.* Quantum Phase Transitions in the Shapes of Atomic Nuclei // Rev. Mod. Phys. 2010. V. 82. P. 2155–2212.
3. *Iachello F.* Dynamic Symmetries at the Critical Point // Phys. Rev. Lett. 2000. V. 85. P. 3580–3583.
4. *Iachello F.* Analytic Description of Critical Point Nuclei in a Spherical-Axially Deformed Shape Phase Transition // Phys. Rev. Lett. 2001. V. 87. P. 052502.
5. *Casten R. F., Zamfir N. V.* Evidence for a Possible $E(5)$ Symmetry in ^{134}Ba // Phys. Rev. Lett. 2000. V. 85. P. 3584–3586.
6. *Casten R. F., Zamfir N. V.* Analytic Description of Critical Point Nuclei in a Spherical-Axially Deformed Shape Phase Transition // Phys. Rev. Lett. 2001. V. 87. P. 052503.

7. *Flocard H. et al.* Nuclear Deformation Energy Curves with the Constrained Hartree–Fock Method // Nucl. Phys. A. 1973. V. 203. P. 433–472.

8. *Ring P., Schuck P.* The Nuclear Many-Body Problem. Berlin: Springer-Verlag, 1980.

9. *Serot B. D., Walecka J. D.* The Relativistic Nuclear Many-Body Problem // Adv. Nucl. Phys. 1986. V. 16. P. 1–321.

10. *Ring P.* Relativistic Mean Field Theory in Finite Nuclei // Prog. Part. Nucl. Phys. 1996. V. 37. P. 193–263.

11. *Meng J. et al.* Relativistic Continuum Hartree–Bogoliubov Theory for Ground-State Properties of Exotic Nuclei // Prog. Part. Nucl. Phys. 2006. V. 57. P. 470–563.

12. *Meng J. et al.* Shape Evolution for Sm Isotopes in Relativistic Mean-Field Theory // Eur. Phys. J. A. 2005. V. 25. P. 23–27.

13. *Fossion R., Bonatsos D., Lalazissis G. A.* $E(5)$, $X(5)$, and Prolate to Oblate Shape Phase Transitions in Relativistic Hartree–Bogoliubov Theory // Phys. Rev. C. 2006. V. 73. P. 044310.

14. *Yu M. et al.* Shape Evolution for Ce Isotopes in Relativistic Mean-Field Theory // Intern. J. Mod. Phys. E. 2006. V. 15. P. 939.

15. *Rodriguez-Guzmin R., Sarriguren P.* $E(5)$ and $X(5)$ Shape Phase Transitions within a Skyrme–Hartree–Fock + BCS Approach // Phys. Rev. C. 2007. V. 76. P. 064303.

16. *Guo J.-Y., Fang X. Z., Sheng Z. Q.* Shape Phase Transitions and Possible $E(5)$ Symmetry Nuclei for Ti Isotopes // Intern. J. Mod. Phys. E. 2008. V. 17. P. 539–548.

17. *Yilmaz A. H., Bayram T.* A Detailed Investigation on the Ground-State Nuclear Properties of Even–Even Mo Isotopes by Using the Relativistic Mean Field Approach // J. Korean Phys. Soc. 2011. V. 59. P. 3329–3336.

18. *Yao B.-M., Guo J.-Y.* Systematic Analysis of Shape Evolution for Mo Isotopes with Relativistic Mean Field Theory // Mod. Phys. Lett. A. 2010. V. 25. P. 1177–1186.

19. *Bayram T.* An Investigation on Shape Evolution of Ti Isotopes with Hartree–Fock–Bogoliubov Theory // Mod. Phys. Lett. A. 2012. V. 27. P. 1250162.

20. *Bayram T., Yilmaz A. H.* A Study on Shape of Te Isotopes in Mean Field Formalism. arXiv:1301.2684 [nucl-th].

21. *Nikssic T. et al.* Microscopic Description of Nuclear Quantum Phase Transitions // Phys. Rev. Lett. 2007. V. 99. P. 092502.

22. *Bender M., Heenen P.-H.* Configuration Mixing of Angular-Momentum and Particle-Number Projected Triaxial Hartree–Fock–Bogoliubov States Using the Skyrme Energy Density Functional // Phys. Rev. C. 2008. V. 78. P. 024309.

23. *Yao J. M. et al.* Configuration Mixing of Angular-Momentum-Projected Triaxial Relativistic Mean-Field Wave Functions // Phys. Rev. C. 2010. V. 81. P. 044311.

24. *Rodriguez T. R., Egido J. L.* Triaxial Angular Momentum Projection and Configuration Mixing Calculations with the Gogny Force // Ibid. P. 064323.

25. *Bholoa A. et al.* A New Approach to Potential Fitting Using Neural Networks // Nucl. Instr. Meth. B. 2007. V. 255. P. 1–7.

26. *Athanassopoulos S. et al.* Nuclear Mass Systematics Using Neural Networks // Nucl. Phys. A. 2004. V. 743. P. 222–235.

27. *Mavrommatis E., Gernoth K. A., Clark J. W.* One and Two Proton Separation Energies from Nuclear Mass Systematics Using Neural Networks. arXiv: nucl-th/0509075.

28. *Peterson K. L.* Classification of Cm II and Pu I Energy Levels Using Counter Propagation Neural Networks // Phys. Rev. A. 1991. V. 44. P. 126–138.

29. *Balabin R. M., Lomakina E. I.* Neural Network Approach to Quantum-Chemistry Data: Accurate Prediction of Density Functional Theory Energies // J. Chem. Phys. 2009. V. 131. P. 074104.

30. *Marim L. R., Lemes M. R., Dal Pino A., Jr.* Ground State of Silicon Clusters by Neural Network Assisted Genetic Algorithm // Tho. Chem. 2003. V. 663. P. 159–165.

31. *Latino Diogo A. R. S. et al.* Mapping Potential Energy Surfaces by Neural Networks: The Ethanol/Au(111) Interface // J. Electroanal. Chem. 2008. V. 624. P. 109–120.

32. *Costris N. et al.* A Global Model of Beta(-) Decay Half-Lives Using Neural Networks. arXiv: nucl-th/0701096v1.

33. *David C., Aichelin J.* Neural Networks Applied to Nuclear Physics // Proc. of the 4th Intern. Workshop on Software Engineering, Artificial Intelligence and Expert Systems for High-Energy and Nuclear Physics (AIHENP'95), Pisa, Italy, April 3–8, 1995. P. 709–718.

34. *Stoitsov M. V. et al.* Axially Deformed Solution of the Skyrme–Hartree–Fock–Bogolyubov Equations Using the Transformed Harmonic Oscillator Basis. The Program HFBTHO (v1.66p) // Comp. Phys. Commun. 2005. V. 167. P. 43–63.

35. *Haykin S.* Neural Networks: A Comprehensive Foundation. Englewood Cliffs, NJ, USA: Prentice-Hall Inc., 1999.

36. *Hornik K., Stinchcombe M., White H.* Multilayer Feedforward Networks Are Universal Approximators // Neural Networks. 1989. V. 2. P. 359–366.

37. Neurosolutions. http://www.neurosolutions.com/.

38. *Levenberg K.* A Method for the Solution of Certain Problems in Least Squares // Quart. Appl. Math. 1944. V. 2. P. 164–168.

39. *Marquardt D.* An Algorithm for Least-Squares Estimation of Nonlinear Parameters // SIAM J. Appl. Math. 1963. V. 11. P. 431–441.

40. *Yildiz N.* Layered Feedforward Neural Network Is Relevant to Empirical Physical Formula Construction: A Theoretical Analysis and Some Simulation Results // Phys. Lett. A. 2005. V. 345, No. 1–3. P. 69.